Nanoindentation near the edge

J.E. Jakes
Materials Science Program, University of Wisconsin—Madison, Madison, Wisconsin 53706; and United States Forest Service, Forest Products Laboratory, Madison, Wisconsin 53726

C.R. Frihart, J.F. Beecher, and R.J. Moon
United States Forest Service, Forest Products Laboratory, Madison, Wisconsin 53726

P.J. Resto and Z.H. Melgarejo
Materials Science Program, University of Wisconsin—Madison, Madison, Wisconsin 53706

O.M. Suárez
Engineering Science and Materials Department, University of Puerto Rico—Mayagüez, Mayagüez, Puerto Rico 00681-9044

H. Baumgart
Applied Research Center, Jefferson National Accelerator Facility, Newport News, Virginia 23606; and Department of Electrical Engineering, Old Dominion University, Norfolk, Virginia 23529

A.A. Elmustafa
Applied Research Center, Jefferson National Accelerator Facility, Newport News, Virginia 23606; and Department of Mechanical Engineering, Old Dominion University, Norfolk, Virginia 23529

D.S. Stone[a)]
Materials Science Program, University of Wisconsin—Madison, Madison, Wisconsin 53706; and Department of Materials Science and Engineering, University of Wisconsin—Madison, Madison, Wisconsin 53706

(Received 31 July 2008; accepted 4 November 2008)

Whenever a nanoindent is placed near an edge, such as the free edge of the specimen or heterophase interface intersecting the surface, the elastic discontinuity associated with the edge produces artifacts in the load–depth data. Unless properly handled in the data analysis, the artifacts can produce spurious results that obscure any real trends in properties as functions of position. Previously, we showed that the artifacts can be understood in terms of a structural compliance, C_s, which is independent of the size of the indent. In the present work, the utility of the SYS (Stone, Yoder, Sproul) correlation is demonstrated in its ability to remove the artifacts caused by C_s. We investigate properties: (i) near the surface of an extruded polymethyl methacrylate rod tested in cross section, (ii) of compound corner middle lamellae of loblolly pine (*Pinus taeda*) surrounded by relatively stiff wood cell walls, (iii) of wood cell walls embedded in a polypropylene matrix with some poorly bonded wood–matrix interfaces, (iv) of AlB_2 particles embedded in an aluminum matrix, and (v) of silicon-on-insulator thin film on substrate near the free edge of the specimen.

I. INTRODUCTION

The most widely used analysis for generating hardness and modulus data from nanoindentation measurements is the method of Oliver and Pharr.[1] Three implicit assumptions behind the method are that the material being tested has rigid support, that it fill a half-space, and that it be homogeneous. When these assumptions are satisfied, the long-range elastic displacements can be estimated based on a Sneddon-type theory for indentation of an elastic half-space by a cone.[2–4] When these assumptions are not satisfied—which is the case for most of the interesting specimens studied these days—Sneddon's theory breaks down, and the utility of the Oliver–Pharr analysis becomes compromised. For instance, many specimens possess two or more phases, and it is of interest to assess the properties of the phases up close to the boundaries between them. However, as we have recently shown,[5] the mere presence of a nearby boundary will cause the properties to appear to change as measurements are placed closer to the boundary, having nothing to do with any real changes in properties. Similar artifacts are encountered if the specimen flexes or has compliant support.

[a)]Address all correspondence to this author.
e-mail: dsstone@wisc.edu
DOI: 10.1557/JMR.2009.0076

Our interest concerns artifacts caused by boundaries and edges. For the present purposes, an edge is where a boundary between the phase being tested and some other phase (including vacuum) intersects the specimen surface. Systems of interest are illustrated in Fig. 1. Figure 1(a) shows a nanoindent placed near an edge of the specimen, corresponding to the "free edge" problem. It is a special case of the more general edge problem, Fig. 1(b), in which the boundary intersecting the surface at right angles separates phases with different elastic properties. Figure 1(c) shows the thin-film geometry, which has been studied extensively in the past (e.g., Refs. 6–9), but which we revisit because we are interested in measurement of properties in a layered specimen near a free edge, Fig. 1(d). Figure 1(e) is an irregular-shaped particle embedded in a surrounding matrix, so the bounding surface is on all sides. A portion of the boundary of the particle might be poorly bonded to the surrounding matrix. Until recently there were no experimental methods to obtain unambiguous nanoindentation data for these types of situations, except for the thin-film geometry case [Fig. 1(c)]. We recently discovered, however, that for nanoindentation in specimens that violate the three assumptions of the Oliver–Pharr method, including the kinds of edge and boundary-related problems represented in Fig. 1, the added complexities can be easily handled by taking into consideration a structural compliance, C_s.[5] The key to the usefulness of C_s is that while it might vary from point to point within the specimen, it can be measured at each point, and to good approximation, is independent of the size of the indent. When C_s is accounted for in the Oliver–Pharr data analysis, the analysis works as well as it would if the experiments were performed on a semi-infinite, rigidly supported, homogeneous specimen. Furthermore, as a by-product of the analysis, C_s is interesting in its own right. For instance, a nearby debonded interface will give rise to a more positive C_s than a bonded interface will, thereby providing the experimenter a way of probing adhesion at an interface.

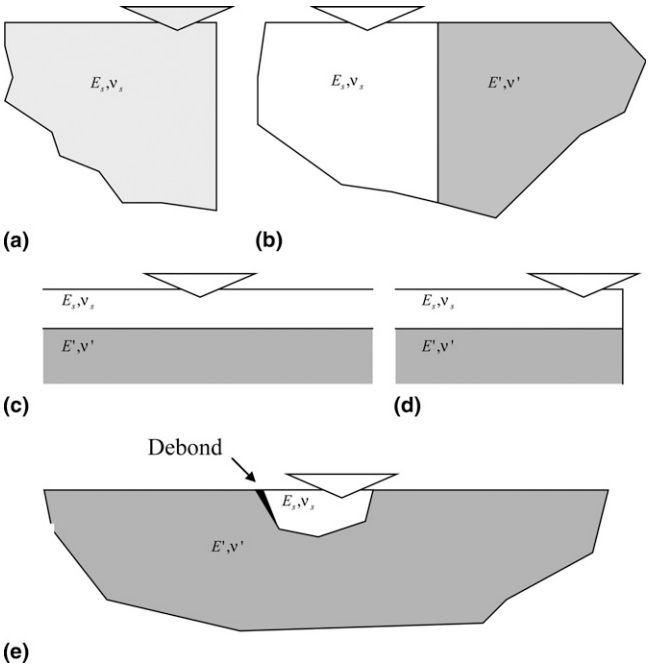

FIG. 1. Some generic edge problems in nanoindentation.

In the present work we build on methods reported previously to explore specimens with edges and boundaries giving rise to C_s. The specimens span a wide breadth of material research topics. Specifically, we investigate (i) a polymethyl methacrylate (PMMA) rod in cross section near the extruded surface, (ii) compound corner middle lamellae (CCML) of loblolly pine (*Pinus taeda*), (iii) wood cell walls in a wood–polypropylene composite, (iv) AlB_2 particles in an aluminum–AlB_2 composite, and (v) a layered silicon-on-insulator (SOI) specimen near a free edge.

II. NANOINDENTATION ANALYSES

A. Standard Oliver–Pharr analysis

With the Oliver–Pharr method,[1] the area of a nanoindent, A, is determined based on contact depth, h_c, defined as

$$h_c = h_0 - \epsilon P_0 C_p \quad , \tag{1}$$

where h_0 is the depth immediately prior to unloading, ε a geometric constant approximately equal to 0.75 for a Berkovich indenter, P_0 is the load immediately prior to unloading, and C_p is the contact compliance, which is the compliance attributable to the specimen and indenter tip. The area of the indent is calculated using h_c in a calibrated area function $A(h_c)$, which depends on indenter shape. In a nanoindent, the Meyer's hardness (H) is

$$H = \frac{P_0}{A} \quad . \tag{2}$$

C_p can be related to specimen and indenter properties using

$$C_p = \frac{1}{E_{eff} A^{1/2}} \quad , \tag{3}$$

where E_{eff} is an "effective" modulus for contact. For indentation against a homogeneous, isotropic, elastic half-space,

$$\frac{1}{E_{eff}} = \frac{1}{\beta}\left(\frac{1-\nu_s^2}{E_s} + \frac{1-\nu_d^2}{E_d}\right) \quad , \tag{4}$$

where E_s and E_d are Young's moduli and ν_s and ν_d are Poisson's ratios of specimen and indenter, respectively. β is a numerical factor, which is usually assumed to be

$2/\pi^{1/2} = 1.128$. Other authors[4,10–12] have reported that this value is too low and that the actual value is closer to 1.2. Finite element analysis simulations of cone indentation in rate-sensitive materials reveal β ranges between 1.16 and 1.22 depending on hardness/modulus ratio.[13] At present, we find that $\beta \cong 1.23$ works best in experiments[5] and therefore use $\beta \cong 1.23$ in both the "standard" analysis, as described in this section, and our "corrected" analysis, described in the next section. If the half-space is layered, then the first term in parentheses in Eq. (4) must be replaced by $1/E_r$, where E_r depends on the size of the indent in relation to the layer thickness.[8]

B. Corrected analysis accounting for structural compliance

Jakes et al.[5] demonstrated that free edges and heterophase interfaces perpendicular to the indentation surface give rise to a structural compliance, C_s, which if not accounted for produces artifacts in the standard analysis. A physical argument to explain the existence of C_s in association with the edge problem is given in the Appendix. Table I summarizes the different types of compliances in a nanoindentation experiment. The machine compliance, C_m, is independent of the size of the indent, positive in value, and a property of the instrument. C_s is also independent of the size of the indent, but it can be positive or negative in value, and can vary sensitively as a function of position within a specimen. In addition to arising from edges, C_s can originate from long-range elastic displacements in a specimen that flexes, such as a cantilever beam under load. To accurately determine C_p for indents placed near the boundaries illustrated in Fig. 1, the sum of the external compliances, $C_m + C_s$, must be calculated and accounted for using the analysis method of Jakes et al.[5] This method simultaneously accounts for C_s arising from both edge effects and long-range elastic displacements by employing the SYS (Stone, Yoder, Sproul)[14] correlation given by

$$C_t P_0^{1/2} = (C_m + C_s) P_0^{1/2} + J_0^{1/2} \quad . \qquad (5)$$

Here, $J_0 = H/E_{eff}^2$ is the Joslin–Oliver[15] parameter. If J_0 and $C_m + C_s$ are independent of load, then $C_t P_0^{1/2}$ plotted as a function of $P_0^{1/2}$ forms a straight line of slope $C_m + C_s$. The intercept, $J_0^{1/2}$, is an area-independent material parameter that represents the ratio $H^{1/2}/E_{eff}$. When the value of C_s could change with location, it is necessary to determine $C_m + C_s$ independently for each indent using either multiload indents or dynamic stiffness measurements.[11] Once $C_m + C_s$ has been determined, then the load–depth trace can be corrected, and A can be calculated based on h_c using the usual Oliver–Pharr approach, but we usually find it advisable to also determine A directly from images of the residual indent. This determination provides a check of A, which is independent of experimental uncertainties associated with detection of the surface, thermal drift, distortion of the indent caused by surface topography and tilt, sink-in, and pileup. Others[16,17] have demonstrated that the area measured after the indenter has been removed is the same as the area at P_0. To test whether the areas of indents shrink following experiments in PMMA, which has a viscoelastic response, we repeatedly measured the profile of an indent at different times between 2 min and 5 days following a test and found that the indent gradually becomes shallower, but its lateral dimensions remain the same. In what follows, the "corrected" analysis will consist of calculating C_p by properly accounting for $C_m + C_s$, determining A by measuring areas from images of residual indents, and using Eqs. (2) to (4) to calculate H and E_s.

When J_0 is dependent on load, such as encountered in a layered specimen or a material that exhibits an indentation-size effect, the constructed SYS correlation will not be a straight line. The SYS correlation can still be used to account for the structural compliance near an edge by modeling the contact compliance and experimentally determining the SYS correlation away from the edge. We will demonstrate how this can be accomplished for nanoindents placed next to the edge of a multilayered specimen. Alternatively, the zero-load limit, where the SYS correlation is extrapolated to $J_0^{1/2}$ ($P_0 = 0$), can be used to determine J_0 for the material at the surface. This value will also be independent of C_s.

TABLE I. Summary of compliances present in a nanoindentation experiment.

Compliance type	Notation	Descriptions
Total	C_t	Measured unloading compliance, obtained from an experimental load–depth trace
Machine	C_m	Compliance attributable to displacements of nanoindenter load frame Machine-dependent
Structural	C_s	Compliance attributable to edge effects or long range elastic displacements within the specimen, as opposed to the displacements caused by a Sneddon-type stress field Dependent on specimen shape, size, support, and homogeneity
Contact	$C_p = (C_t - C_m - C_s)$	Indenter-specimen compliance in the absence of structural compliance; its value can be obtained from Sneddon-type elasticity solution for indentation by a cone or pyramid indenter against a rigid half-space

III. EXPERIMENTAL WORK

This work investigates nanoindentation in specimens that possess nearby structural heterogeneities such as free edges and heterophase interfaces, features that produce artifacts in the measurement of local properties when standard nanoindentation methods are used. Only after these artifacts are removed can potential changes in material properties near these heterogeneities be studied. The specimens listed in Table II all possess different kinds of structural heterogeneities, either as single features or combinations of features. For specimens 1 to 4, the artifacts introduced by the structural heterogeneities can be corrected using the concept of a C_s, which can be either positive or negative and which depends on position of the indent relative to the heterogeneities. For these specimens the SYS plot is a straight line, and C_s can be determined from the slope of that line. Specimen 5 is different. It possesses thin-film geometry with the thin-film layers parallel to the surface, and because of this the SYS plot is no longer a straight line. The line is curved, yet elasticity theory can be used to model its shape. The solution to the layered problem has been studied for many years dating back to Doerner and Nix[7] and King.[6] The present work addresses the added complexity of an indent placed near the free edge of the layered specimen.

A. Specimens

Specimen 1 is a 3.33 mm diameter extruded polymethyl methacrylate (PMMA) rod (density 1.15 g/cm^3) obtained from Cope Plastics, Inc. (Godfrey, IL). A 3 mm thick cylinder was removed from the end for testing and cross-sectioned perpendicular to the extrusion direction using an ultramicrotome fit with a diamond knife. The mechanical properties of the material near the extruded surface were investigated by placing indents close to the free edge formed by the extruded surface (Fig. 2). To serve as a control, an additional free edge was created by an ultramicrotome fit with a glass knife in the middle of the cross-sectioned rod (Fig. 2) so that properties could be tested without influence of the extrusion process. The two different edges are referred to as "extruded" and "microtomed" edges. In addition, indents were placed in the middle of the specimen to test properties without influence of the edges.

For us, specimen 1 serves as a model system to develop protocols for investigating the measurement of creep properties near edges. Our ultimate goal is to investigate the creep properties of the wood cell wall, where edges are always close by. For this reason, the load–depth profiles used in the experiments on PMMA contain segments that are associated with the creep tests, described in more detail below. Analysis of the creep segments is the subject of a future paper. Nevertheless, the fact that the hardnesses reported below come from the creep portion of the experiments, while the $J_0^{1/2}$ values come from the multiload portion of the experiments means that some inconsistencies will seem to exist between the different versions of the data. We shall point out these apparent inconsistencies when they arise. They come entirely from differences in indentation creep rate and do not materially affect the conclusions drawn from these experiments.

Specimen 2 is the compound corner middle lamella (CCML) in the transverse plane of latewood in plantation-grown loblolly pine (*Pinus taeda*). The CCML is a continuation of middle lamellae, which holds cells together, into the junction between three or more wood cells. It is more compliant than the cell walls surrounding it, and indents placed in the CCML will possess a negative C_s. The specimen surface was prepared using a diamond knife in an ultramicrotome without the aid of polymeric embedments that might otherwise have altered the properties of the wood. Such embedments make the specimen more rigid and therefore decrease the effects of artifacts caused by edges, but with our methods those artifacts are removed. Additional detail about the specimen preparation is given in an earlier publication.[5]

Specimen 3 consists of wood cell walls embedded in a polypropylene matrix. An ultramicrotome fit with a diamond knife was again used to prepare the specimen surface, and additional details about the specimen and surface preparation are given in Ref. 5. The cell walls were tested in transverse cross section, and here the surrounding matrix, in contrast to specimen 2, is more compliant than the material being tested. Complicating

TABLE II. Summary of specimens investigated.

No.	Specimen	Interface orientation with respect to indentation surface	Approximate specimen geometry (Fig. 1)	Nanoindenter	Imaging
1	PMMA	Perpendicular	1(a)	Hysitron Triboindenter	AFM
2	CCML	Perpendicular	1(b), 1(e)	Hysitron Triboindenter	AFM
3	Wood cells	Perpendicular	1(a), 1(b), 1(e)	Hysitron Triboindenter	AFM
4	AlB_2	Random	1(e)	Hysitron Triboscope	SEM
5	SOI	Parallel (layers) and perpendicular (edge)	1(c), 1(d)	Hysitron Triboindenter MTS Nanoindenter XP	AFM N/A

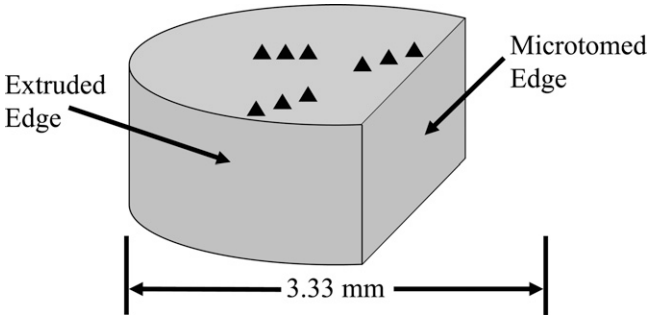

FIG. 2. Sample preparation of PMMA specimen. Groups of triangles represent the three areas where arrays of indents were placed: in the bulk, near the extruded edge, and near the microtomed edge.

the geometry is the presence of a number of cracked cell walls and cracked wood–polypropylene interfaces. These complications are easily accounted for using the corrected analysis.

Specimen 4 consists of 3 to 10 μm sized AlB_2 particles embedded in an aluminum matrix. The composite was manufactured[18–20] from an Al and 5 wt% B master alloy from Milward Alloys, Inc. (Lockport, NY). The nanoindentation surface was ground using successive grit sizes of 320, 400, 600, 800, and 1200 SiC paper. Additional polishing was performed with a 3 μm SAMTE DP diamond suspension and DEPPO DP lubricant mixed on a MD-MOL cloth and after that, a MD-CHEM cloth wetted with a colloidal silica suspension. All these products are produced by Struers Inc. (Westlake, OH). Finally, the surface was subjected to ultrasonic cleaning. With hp3 hexagonal crystal structure, AlB_2 is transversely anisotropic in its elastic properties and is also expected to be anisotropic in its hardness properties. We are interested in calculating the "orientation-dependent" properties of the AlB_2 phase independent of the surrounding matrix. To identify the orientation of the polished surface indented, electron beam backscattering analysis (EBSD) in a Leo (Oberkochen, Germany) Gemini 1530 scanning electron microscope (SEM) was used.

Specimen 5 is a relaxed silicon-on-insulator (SOI) specimen prepared through SMART CUT technology. The specimen consists of a 65 nm thick relaxed silicon layer on top of an insulating, 149 nm thick silicon oxide layer, which is deposited on top of a 525 μm thick silicon wafer of 100 orientation. The thicknesses of the two top layers were measured by a Woollam (Lincoln, NE) ellipsometer. Further details about this specimen are given by Miller et al.[21] In the analysis of this specimen, elasticity theory was used to model the effects of the different layers on measured stiffness. Some of the indents were placed near the free edge of the specimen to examine the combined effects of layers and free edge. The free edge was prepared by cleaving the specimen along a 100 surface.

B. Nanoindentation procedure

Three commercial nanoindenters were used in this study. A Hysitron (Minneapolis, MN) Triboindenter was used to investigate specimens 1 to 3 and 5. An MTS (Oak Ridge, TN) Nanoindenter XP was also used to investigate specimen 5, and a Hysitron Triboscope was used in the experiments on specimen 4. All nanoindenters were equipped with Berkovich tips, and standard methods were used to calculate the machine compliance and area function (based on contact stiffness) using series of indents in the center of fused silica standards. However, the area function for the Hysitron Triboindenter was calculated using $\beta = 1.23$[5] instead of $\beta = 1.128$, which is used more often in the literature.[1,7] To construct the SYS correlations necessary for our data analysis, unloading stiffness must be calculated as a function of load. For the MTS Nanoindenter XP, this is accomplished by performing experiments using the continuous stiffness measurement (CSM) technique.[11] For the Hysitron nanoindenters, this was accomplished by using multiload indents, which consisted of loading segments, holds at partial loads, unloading segments, and holds at the partial unloads with the load increasing for each cycle. A partial unload held for 60 s was also included to calculate thermal drift. The multiload indent load function was different for each of the specimens in this work, with varying numbers of cycles and segment times. An example is given in Fig. 3, showing the load function (inset) and the resulting load–depth trace obtained from a multiload indent performed on a CCML using the Hysitron Triboindenter.

Young's moduli (E_s) of the materials in this study were calculated using Eq. (4), where E_d and ν_d for the diamond tip were assumed to be 1137 GPa and 0.07, respectively. The values of Poisson's ratio used for cell walls, CCML, and PMMA were 0.45,[22] 0.45,[22] and 0.35, respectively.

C. Area measurement using AFM and SEM

For experiments performed with the Triboindenter, residual indents were imaged with a Quesant (Agoura Hills, CA) atomic force microscope (AFM) incorporated in the Triboindenter. The AFM was operated in contact mode and calibrated using an Advanced Surface Microscopy, Inc. (Indianapolis, IN) calibration standard with a pitch of 292 ± 0.5 nm. Successive scans and calibration routines revealed the reproducibility of the AFM calibration to be ±1%. Each scan size used was independently calibrated. Individual 10 μm field-of-view images were made of each indent in specimen 1, and 4 μm field-of-view images were made of each indent in specimens 2, 3, and 5. Both z-height and lateral force images were analyzed as described previously.[5] The residual indents of experiments performed with the Triboscope were

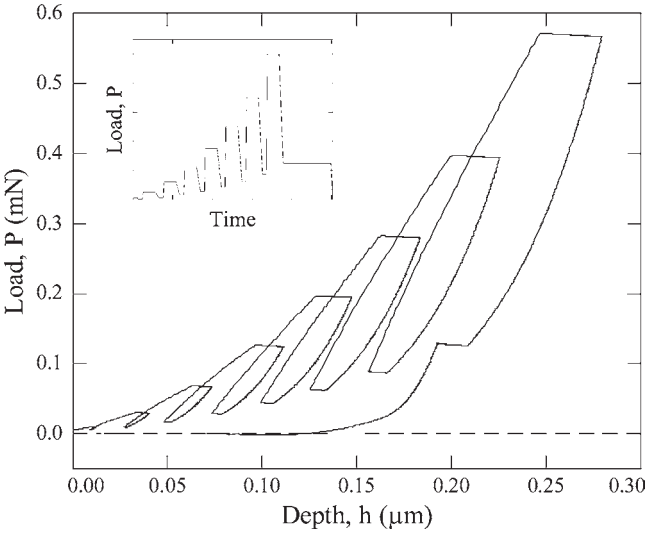

FIG. 3. Load–depth trace of a multiload indent on CCML in latewood of loblolly pine. Insert shows the load function used to create this indent, consisting of 1 s loading segments, 15 s holds at partial loads, 5 s unloading segments, and 5 s holds at the partial unloads. There were seven loading segments that loaded to 5, 12, 22.5, 35, 50, 70, and 100% of the final maximum load. Each partial unload was to 25% of the previous partial load, and the final partial unload was held for 60 s to calculate thermal drift before complete unloading. The hysteresis seen in the unloading–reloading segments is caused by viscoelastic rebound.

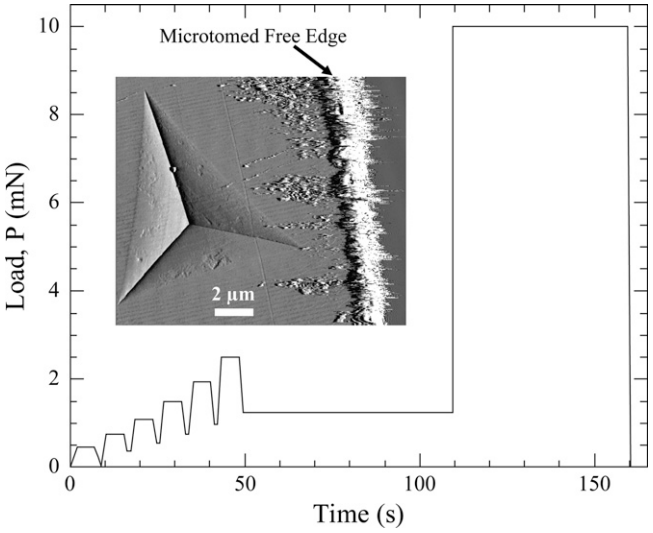

FIG. 4. Load function used for 10 mN indents on PMMA. Inset: AFM image of 10 mN indent placed near microtomed edge in PMMA. The SYS plots (Fig. 6) were constructed from the multiload portions of the indents, at which point the indents were only about one half as large in diameter as the final indent shown in the inset.

imaged using a calibrated Leo (Oberkochen, Germany) Gemini 1530 scanning electron microscope (SEM) capable of full orientation imaging based on EBSD Kikuchi patterns. EBSD was used to determine the crystallographic orientation of the AlB_2 particles tested by nanoindentation. ImageJ (http://rsb.info.nih.gov/ij/) image analysis software was used to manually measure the projected contact areas from both the AFM and SEM images. Indents made with the Nanoindenter XP were not imaged. Instead, the areas were calculated based on contact depth.

IV. RESULTS AND DISCUSSIONS

A. Edge effect in PMMA specimen

To study the properties near the edges of the PMMA specimen, 10 mN multiload indents were placed in three separate locations (Fig. 2). Sixteen indents were placed between 5.7 and 75.2 μm of the extruded free edge, 16 indents were placed between 7.5 and 80.3 μm of the microtomed free edge, and 3 indents were placed in the bulk region of the PMMA far from the edges. Distances d were, as always, measured from the centers of the indents to the free edge. Figure 4 shows the loading profile used for the PMMA indents along with an AFM image of an indent placed near the microtomed free edge. As discussed previously, the first six loading segments are used for constructing the SYS plot to calculate

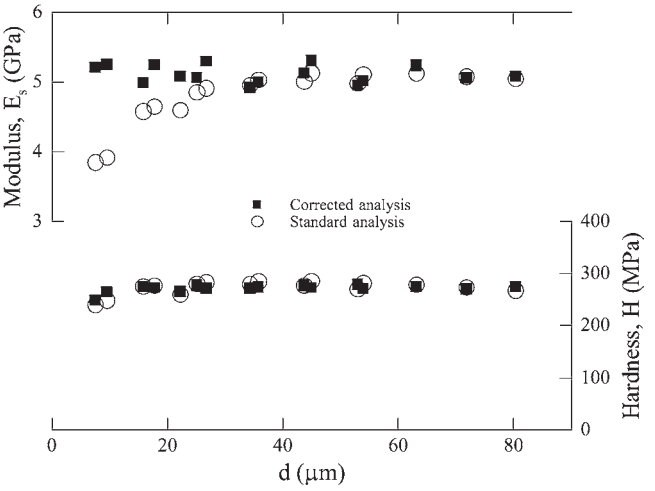

FIG. 5. Values of E_s and H calculated for standard and corrected analyses for indents performed near the microtomed edge of PMMA specimen. The distance to the edge (d) is measured from the center of the indent to the free edge.

C_s, whereas the last segment is used to conduct a nanoindentation creep experiment. Hardness and modulus were calculated using both standard and corrected analyses for the final unloading segment. Figure 5 shows the resulting E_s and H values for indents placed near the microtomed free edge. The values of E_s and H calculated from the standard analysis assume $C_s = 0$ and $C_m = 2.7$ μm/N. When calculated using the standard analysis, both E_s and H appear to decrease as the free edge is approached.

The SYS correlations for these indents are displayed in Fig. 6. No appreciable indentation size effect in the hardness or modulus of PMMA is evident, so the fact

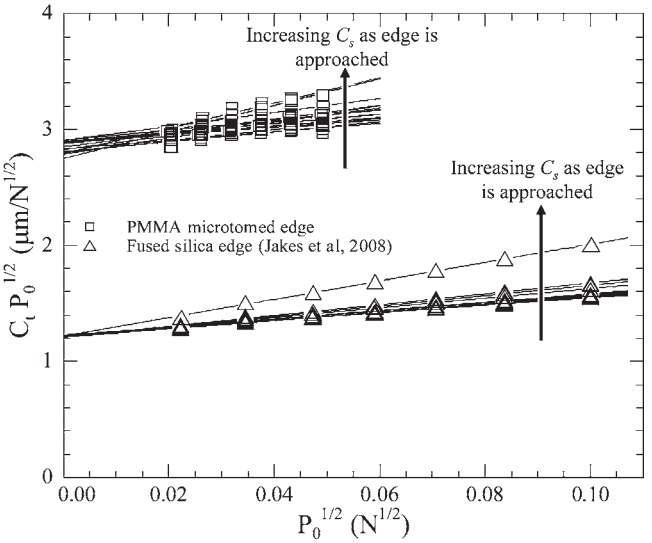

FIG. 6. SYS correlations for multiload indents near microtomed PMMA edge and edge of fused silica standard from Ref. 5.

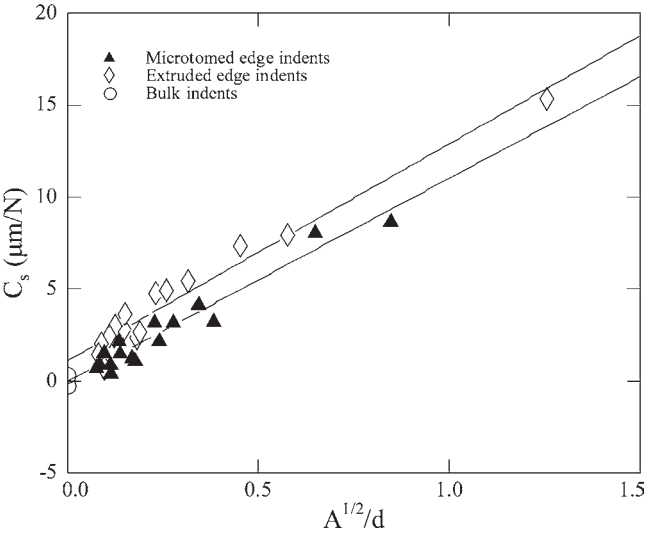

FIG. 7. Relationship between C_s and the distance (d) measured form the center of the indent to the microtomed or extruded edges in the PMMA specimen. The bulk indents are plotted at $A^{1/2}/d = 0$.

that the SYS plots possess slopes higher than C_m= 2.7 μm/N demonstrates the existence of a structural compliance, C_s [Eq. (5)]. The indents placed nearer the edge possess higher slopes, which indicate that C_s increases as the edge is approached. Also included in Fig. 6 are the SYS correlations for fused silica near a free edge presented earlier.[5] The different intercepts, $J_0^{1/2}$ = 2.85 ± 0.05 μm/N$^{1/2}$ for PMMA and $J_0^{1/2}$ = 1.218 ± 0.007 μm/N$^{1/2}$ for fused silica, arise because the two materials have different properties. We compare the two sets to demonstrate that the scatter in $J_0^{1/2}$ is larger for the PMMA, which indicates that the PMMA specimen is less uniform in its properties than is the fused silica.

If the hardness and modulus values in Fig. 5 are used to calculate $J_0^{1/2}$, the result is 2.31 μm/N$^{1/2}$, which is about 20% lower than the intercept for the PMMA data in Fig. 6. This difference is caused by differences in indentation strain rates in the two portions of the load function (Fig. 4). Indentation strain rate is defined in Ref. 13. In the first portion of the load function, containing the six cycles used to construct the SYS correlation, the holds at partial loads are all 5 s long and the indentation strain rates at the ends of the segments are all about the same, resulting in a constant hardness. In the second portion, or final cycle, of the experiment the hold is 50 s and as a consequence, the indentation strain rate at the end of this segment is about a factor of 10 lower than that for the six partial loads. The hardness of PMMA is sensitive to strain rate, so the hardness after the 50 s hold is lower, which is why the value of $J_0^{1/2}$ is lower when calculated from the hardness and modulus in Fig. 5.

Jakes et al.[5] used dimensional analysis to argue that C_s caused by a nearby free edge should have the general form

$$C_s = \frac{1}{Md} f\left(\frac{A^{1/2}}{d}\right) \quad , \tag{6}$$

where M is the relevant elastic modulus, d is the distance from the center of the indent to the free edge, and f is some function. Experiments on fused silica suggested that f is approximately a constant, even for large $A^{1/2}/d$ (i.e., close to the edge). Theoretical work by Gerber[23] supports the same conclusion.[5] To test this relation for PMMA we plot C_s against $1/d$ in Fig. 7. The bulk indents are assumed to be an infinite distance from the edge ($1/d$ = 0). The straight line fits to the two sets of edge data are consistent with our earlier findings for fused silica and support that f in Eq. (6) is nearly constant. The intercepts for the two sets of edge data differ by about 1 μm/N, which is likely caused by slight differences in the long-range flexing of the specimen depending on where the indents are placed. This flexing introduces an additional source of C_s. The ability to detect this difference between the two sets of data reveals how sensitive the method can be. The data from the microtomed edge extrapolate directly to $C_s \approx 0$ μm/N, in agreement with C_s measured for the bulk indents. In Fig. 5 the unaccounted-for C_s in the standard analysis is responsible for the differences between the standard and corrected analyses. Using the corrected analysis we find that E_s is unaffected by the microtomed edge and H is only slightly lowered in the case of the closest indent. Similarly, using the corrected analysis we find that E_s is not affected by the extruded edge and H is lowered for the closest indents (Fig. 8). Without using the corrected methods, both E_s and H would have appeared to substantially decrease near the edges. Overall, E_s = 5.1 ± 0.1 GPa was calculated for this PMMA specimen and the presence of nearby free edges had no detectable effect.

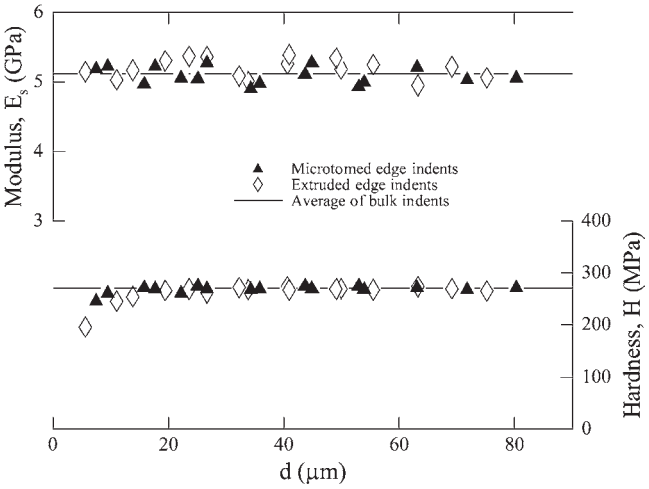

FIG. 8. Values of E_s and H calculated using the corrected analysis for indents performed near the microtomed and extruded edges of the PMMA specimen. The distance to the edge (d) is measured from the center of the indent to the free edge. The extruded edge shows a larger decrease in hardness near the edge (extruded surface) compared to the microtomed edge.

The average H for the indents far from the edge ($d > 15$ μm for both edges and the bulk indents) was 270 ± 10 MPa. The closest indent for the microtomed edge, d = 7.5 μm, had H of 250 MPa and for the closest indent near the extruded edge, d = 5.7 μm, H dropped to 200 MPa. It is notable that these changes in H were detected directly from changes in areas measured from AFM images and are independent of the determination of C_s.

The origins of the decrease in H near the microtomed and extruded edges remain unclear. It is possible that they are artifacts arising from plastic zone-size effect. We previously observed that for fused silica H remains unchanged for indents placed as close as $0.8A^{1/2}$ of the edge.[5] However, the size of the plastic zone under the indenter varies inversely with the ratio of hardness to elastic modulus,[24,25] and because this ratio is about three times smaller for PMMA than it is for fused silica, we would anticipate that the effect of the edge on H extends further in PMMA than in fused silica. The exact mechanisms causing the decreases in H near the edges in PMMA are not yet fully understood, but the experiments demonstrate that there is a larger decrease in H near the extruded edge than the microtomed edge.

B. Compound corner middle lamella of loblolly pine

In most biological materials, including wood, the features of interest have dimensions on the order of micrometers. To investigate the properties of these features using nanoindentation, the effects of nearby elastic discontinuities must be taken into account. At the micrometer level, wood is primarily composed of hollow cells held together by a material called the middle lamella,

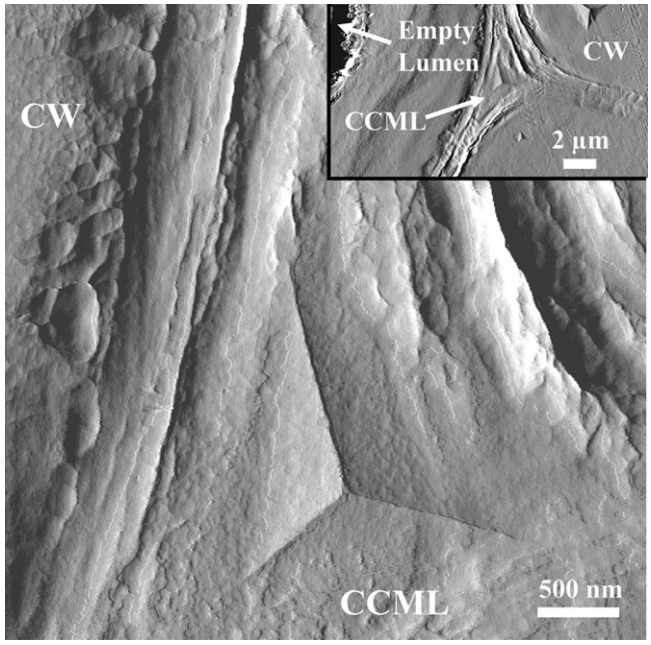

FIG. 9. AFM images of an indent in a compound corner middle lamella (CCML) of latewood in loblolly pine. CCML form in the junction of three or more cell walls (CW).

and understanding the individual properties of the cell wall and middle lamella preludes a comprehensive understanding of bulk wood. Structurally and chemically, the cell walls and middle lamellae are quite different. The cell walls consist of a nanofiber-reinforced composite with cellulose microfibrils embedded in a matrix of hemicellulose and lignin subdomains. The middle lamellae are composed primarily of lignin, an amorphous, highly cross-linked aromatic biopolymer. The middle lamelle layer between two adjacent cells is thin (~200 nm), but at the junction of three or more cells, a larger middle lamella (~2 μm) area is formed (inset of Fig. 9), called the compound corner middle lamella (CCML). These larger areas are suitable for nanoindentation experiments; however, they are surrounded by stiffer cell walls. The CCML appears to be well adhered to the cell wall.

Using the Triboindenter, 0.6 mN multiple load indents were performed in three separate CCML in the transverse plane of the latewood region of a loblolly pine specimen. The AFM image of one residual indent is displayed in Fig. 9. The resulting SYS correlations are shown in Fig. 10. The slopes, representing $C_m + C_s$ = −2 ± 2 μm/N, are indicative of a negative structural compliance caused by the CCML being well adhered to the nearby stiffer cell wall. ($C_s \approx -5 \pm 2$ μm/N because C_m = 2.7 μm/N; the concept of a negative structural compliance is discussed in more detail in the Appendix.) Using the corrected analysis, the E_s and H for the CCML are calculated to be 5.0 ± 0.1 GPa and 420 ± 20 MPa, respectively. The standard analysis gives 5.2 ± 0.2 GPa

and 400 ± 70 MPa, respectively, so in this case the modifications introduced by the corrections are small. The reason these corrections are small in this case is that the indents themselves are small (0.6 mN), and compliance corrections become negligible as indents are made vanishingly small. The negative C_s arises from the higher stiffness of the nearby latewood cell walls, which for these experiments were found to have an $E_s = 10 \pm 1$ GPa. Previously, we found $E_s = 19 \pm 1$ GPa,[5] for similar cell walls; however, when the present experiments were performed, the relative humidity (RH) was about 50%, compared with 20% for the earlier experiments. The higher RH means more water is present in the cell walls, which in turn causes a plasticizing effect and lowers the Young's modulus. We would anticipate that if the CCML were tested at lower humidity, then C_s would increase because of the increase in modulus of the surrounding cell walls. It would be necessary to account for the changing C_s to accurately determine changes in properties of the CCML with changing RH.

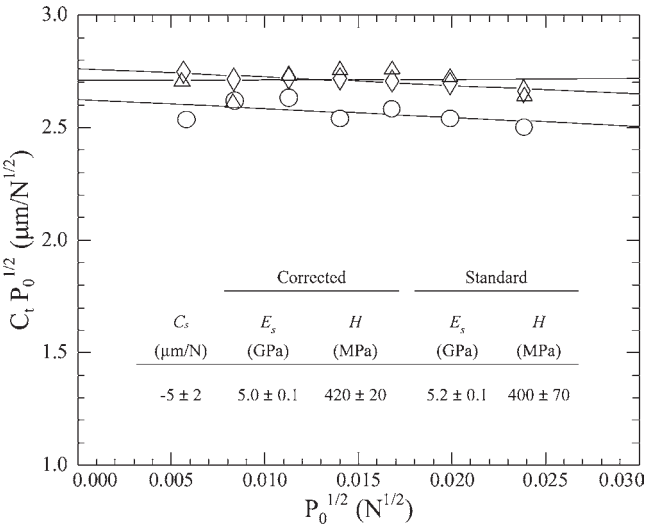

FIG. 10. SYS correlations and tabulated results for indents placed in CCML.

C. Wood cell walls in wood–polypropylene composite

A survey of the prepared wood–polypropylene composite reveals damaged wood cells (Fig. 11). Potential sources of C_s in the wood cell walls include cracks, both within the cell walls and between the cell walls and surrounding matrix, and relatively compliant polypropylene matrix itself, which has a Young's modulus of 2.7 ± 0.2 GPa.[5] Figure 11 shows indents placed in three separate fragments of cell wall labeled with a circle, triangle, and square, respectively. The corresponding data are labeled by the same shapes in Fig. 12. Using the standard analysis, it appears that the mechanical properties of the three cell wall fragments are different. For example, the fragment labeled with a triangle has the lowest E_s value (6.4 ± 0.7 GPa) and the fragment labeled with a circle the highest (8.7 ± 0.4 GPa). However, the fact that the SYS plots all have the same intercept in Fig. 12 suggests that the standard analysis is wrong, and that, instead, the properties of the cell walls are all about the same. From the SYS plots it becomes clear that apparent differences in hardness and modulus arise instead from differences in C_s. Once these differences in C_s are corrected, the differences in hardness and modulus diminish. We conjecture that the piece of cell wall labeled with a triangle has a larger C_s than the other two pieces because it has more cracks around it.

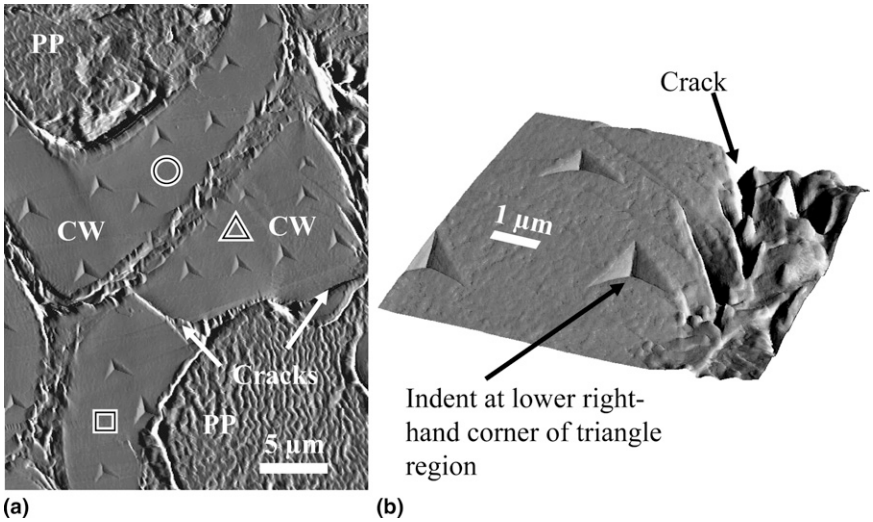

FIG. 11. (a) AFM image of indents placed in wood cell walls (CW) embedded in a polypropylene (PP) matrix. The square, circle, and triangle symbols in this figure refer to Fig. 12 and identify the locations from which the data in that figure were taken. (b) Close-up of indents in the triangle region, showing crack between CW and matrix.

D. AlB_2 particles in aluminum–AlB_2 composite

Aluminum diboride (AlB_2) particles, typically 3 to 10 μm in size, were located by imaging the specimen with the indenter tip of the Hysitron Triboscope. Ten particles were probed with multiload indents, one indent in each particle. The maximum loads ranged from 4 to 8 mN. Indents in two particles are shown in Fig. 13. Because the particles are randomly oriented hexagonal plates, they appear to range in shape from irregular polygons to rectangles to hexagons. From the SYS plots, the structural compliance is estimated assuming that the indentation size effect in hardness is small, a reasonable assumption given the high hardness of AlB_2. SYS plots from four multiload indents are shown in Fig. 14. The straight line fits support that the indentation size effect is small and that C_s is independent of the size of the indent at these loads. Using EBSD we find that $J_0^{1/2}$ correlates with φ, the angle between the crystallographic *c* axis of the diboride and specimen surface (Fig. 15). Elastically,

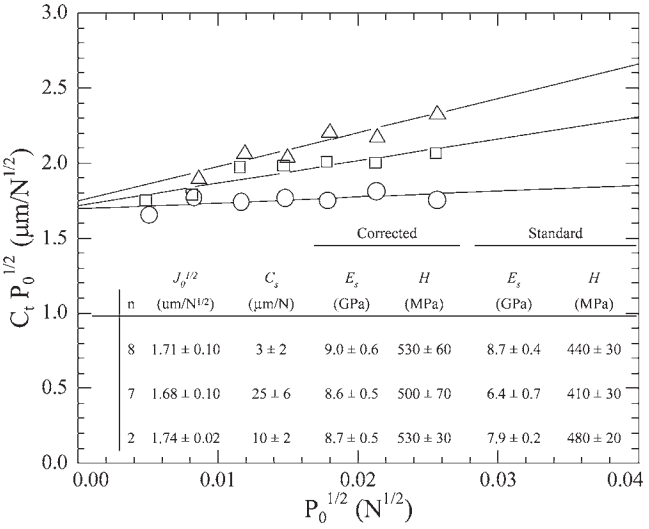

n	$J_0^{1/2}$ (um/N$^{1/2}$)	C_s (μm/N)	E_s (GPa)	H (MPa)	E_s (GPa)	H (MPa)
8	1.71 ± 0.10	3 ± 2	9.0 ± 0.6	530 ± 60	8.7 ± 0.4	440 ± 30
7	1.68 ± 0.10	25 ± 6	8.6 ± 0.5	500 ± 70	6.4 ± 0.7	410 ± 30
2	1.74 ± 0.02	10 ± 2	8.7 ± 0.5	530 ± 30	7.9 ± 0.2	480 ± 20

FIG. 12. Representative SYS correlations, along with values of E_s and H from indents placed in the wood cell walls displayed in Fig. 11. The symbol shapes designate which regions the data came from in Fig. 11.

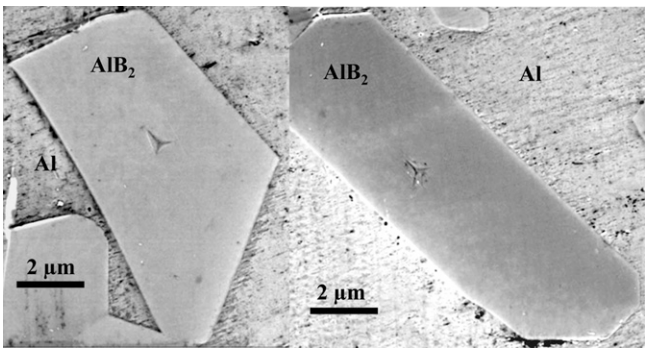

FIG. 13. SEM images of indents placed in AlB_2 particles.

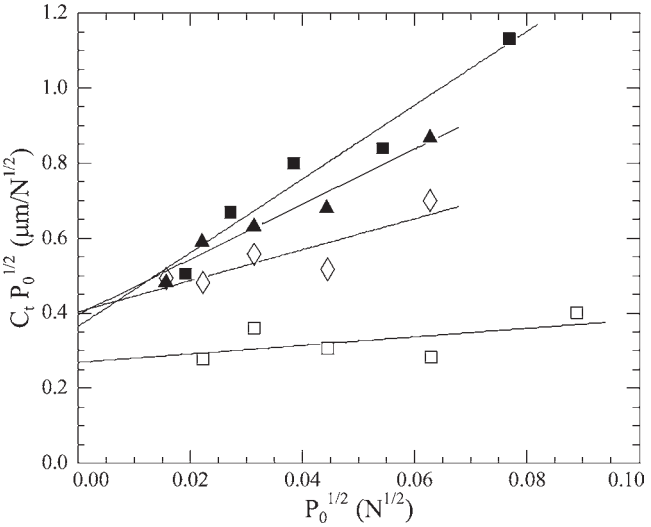

FIG. 14. SYS plots of multiload indents placed in AlB_2 particles.

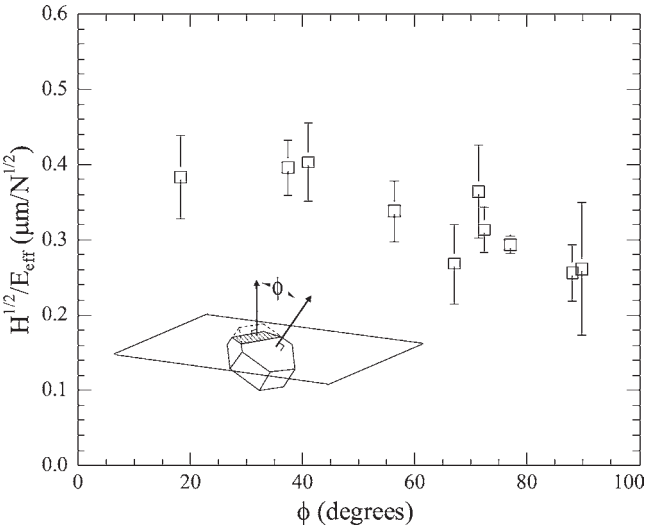

FIG. 15. Dependence of $J_0^{1/2}$ ($H^{1/2}/E_{eff}$) on φ for AlB_2 particles. $J_0^{1/2}$ obtained by SYS intercept. Error bars determined by least square analysis of the lines to the SYS plots. Inset: Schematic defining φ with respect to particle shape.

AlB_2 is transversely isotropic with the *c* direction being the axis of symmetry. Thus, E_{eff} should depend only on φ. The relation between E_{eff} and φ is shown in Fig. 16 for both the uncorrected and corrected analyses. The corrected analysis reveals that E_{eff} increases as φ increases. The standard analysis not only underestimates E_{eff}, but misses the overall trend with φ because the error is larger at high φ than low φ. For comparison with our data, there are no reliable measurements of the elastic constants of isolated AlB_2. However, using a rule of mixtures law, Deppisch et al.[26] estimated a Young's modulus of 450 GPa for AlB_2 flakes based on the Young's modulus of an AlB_2-reinforced alloy. Liu and coworkers[27] recently used ab initio calculations to

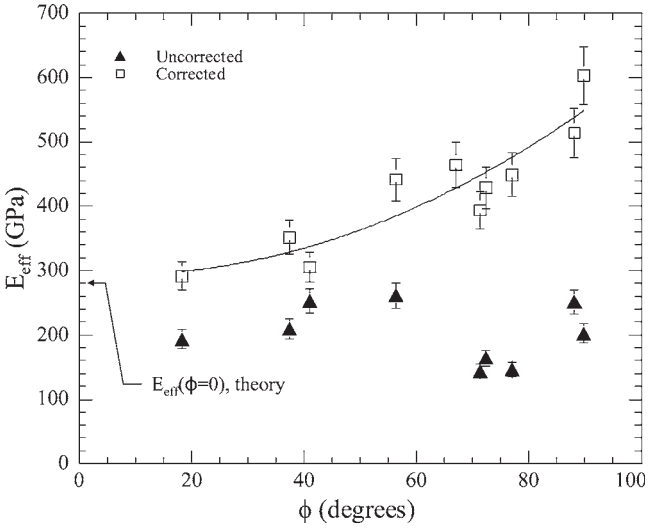

FIG. 16. Dependence of E_{eff} on φ for AlB_2 particles. The theory is based on the contact problem between an indenter and a transversely isotropic solid given by Stone[8] (i.e., AlB_2 with φ = 0) and the elastic constants from Liu et al.[27]

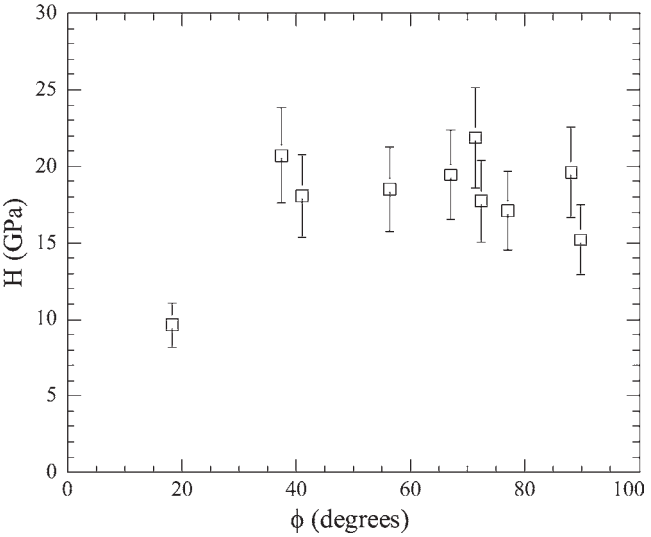

FIG. 17. Dependence of H on φ for AlB_2 particles.

TABLE III. Elastic constants C_{ij} for AlB_2 (in GPa).[27]

	C11	C12	C13	C33	C44
AlB_2	665	41	17	417	58

estimate the elastic constants of AlB_2. Their results are shown in Table III. From elasticity theory for a transversely isotropic solid[8] we can use these elastic constants to estimate E_{eff} = 282 GPa for indentation against the transversely isotropic plane (φ = 0). Our experimental data are consistent with this value. Furthermore, C_{11}, the in-plane elastic stiffness, is higher than C_{33}, the out-of-plane elastic stiffness, which suggests that E_{eff} should increase with increasing φ, which is consistent with our experimental observation. Vlassak and Nix[28] published a method for obtaining the solutions for arbitrary orientations φ. We are in the process of evaluating these solutions for AlB_2.

The measured H values of AlB_2 are shown in Fig. 17. For the most part, the data show a slight increase in going from high to low φ. We anticipate the highest hardness to be observed for φ = 0 given that dislocation slip takes place on the (0001) planes, which have the least resolved shear stress. In this regard, we believe that the single data point at φ = 20° showing unusually low hardness is an outlier, possibly because the plastic zone extended beyond the boundaries of the particle.

E. Silicon-on-insulator (SOI)

The behavior of the SOI is dominated by the presence of heterophase interfaces lying parallel to the indentation surface, which leads to an indentation size effect in E_{eff} and to a lesser extent H. A consequence of this indentation size effect is that the SYS correlations are no longer straight lines. However, the SYS correlation still remains a vital tool in our analysis of nanoindentation data, and within the context of indents placed near an edge, the constant C_s construction remains useful.

SYS correlations obtained from indents made in the center of the specimen with the MTS and Hysitron nanoindenters are displayed in Fig. 18 along with a curve generated from elasticity theory,[8] taking into account the properties of all the layers. The two experimental curves look different because the data were obtained in different ways (continuous stiffness-vs-load measurements from the MTS Nanoindenter and discrete stiffness–load measurements from multiload indents using the Hysitron Triboindenter). The experimental curves in Fig. 18 are corrected for C_m, so they represent $H^{1/2}/E_{eff}$ directly as a function of load for the SOI. For the theoretical simulations, E_{eff} was first calculated as a function of $A^{1/2}$ from elasticity theory, then the calculated E_{eff}-versus-$A^{1/2}$ curve was transformed into a $H^{1/2}/E_{eff}$-versus-$P_0{}^{1/2}$ (= $H^{1/2}A^{1/2}$) curve using hardness as the single fitting parameter to achieve agreement with the experimental data.[9,14] H is of course not constant as a function of load for the indents that pass through the different layers; nevertheless, H for silicon and fused silica are reasonably close (12.5 GPa and 11.1 GPa, respectively[5]) so the assumption H = 11.8 GPa is reasonable for the simulations and allows the overall shape of the SYS curve in Fig. 18 to be approximated based on changes in E_{eff} alone. Note that in Fig. 18, the MTS Nanoindenter XP and Hysitron curves lie almost directly on top of each other, signifying that both instruments are

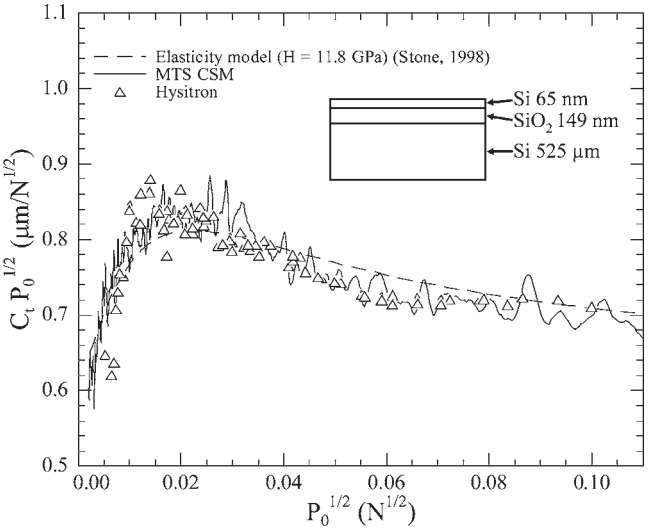

FIG. 18. SYS correlations for indents near the center of the SOI specimen, far from the edge. The basis for the theory curve is described in the text and in more detail in Refs. 8, 9, and 14. Inset: Schematic showing cross section of SOI specimen.

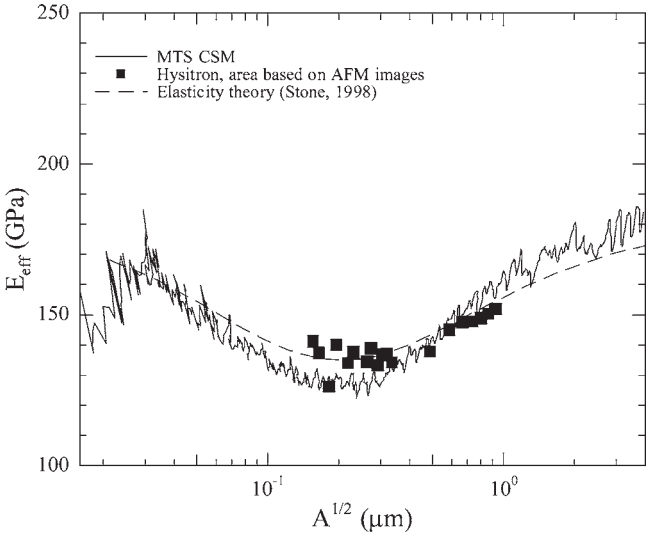

FIG. 20. E_{eff} as a function of $A^{1/2}$ for indents near the center of the SOI specimen, far from the edge. The basis for the theory curve is described in the text and in more detail in Refs. 8, 9, and 14.

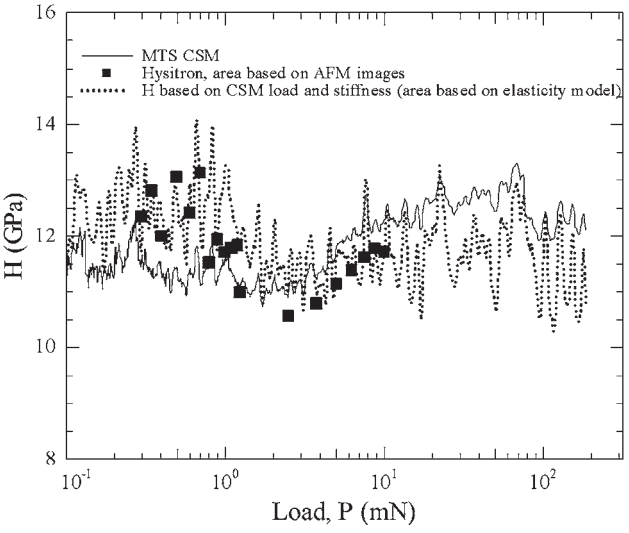

FIG. 19. H as a function of load for indents placed near the center of the SOI specimen, far from the edge. The basis for the theory curve is described in the text and in more detail in Refs. 8, 9, and 14.

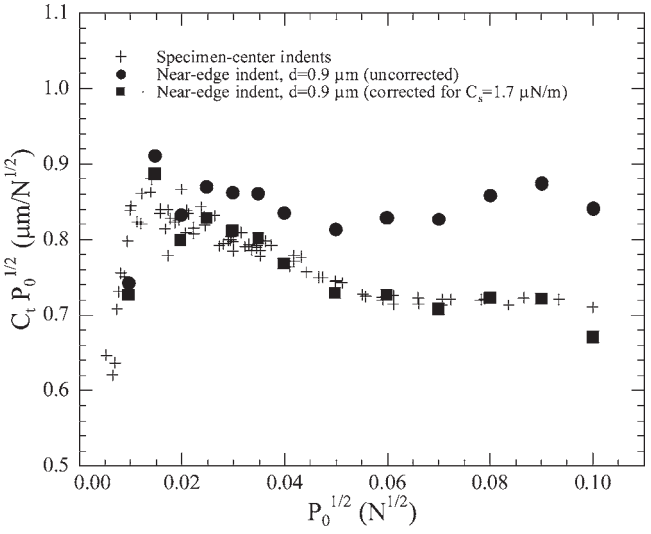

FIG. 21. SYS correlations for multiload specimen-center indents and multiload near-edge indents of the SOI not accounting for C_s ("uncorrected") and accounting for C_s = 1.7 μN/m ("corrected"). The experiments were performed with the Hysitron Triboindenter. For the near-edge indent the data point at the highest load is believed to have been affected by fracture (see Fig. 22).

measuring the same values for the area-independent term $J_0 = H^{1/2}/E_{\text{eff}}{}^2$. In performing the theoretical calculations, we assumed that the Young's moduli of silicon and fused silica are 161 and 72 GPa, respectively, and that the Poisson's ratios are 0.227 and 0.17. $\beta = 1.23$ is used. These values were previously found to work for nanoindentation of the monolithic materials.[5]

The corresponding values of H and E_{eff} are shown in Figs. 19 and 20, respectively. The values of H and E_{eff} obtained from the Hysitron and MTS instruments are slightly different, which can be attributed to differences in the ways the projected areas were determined. Elasticity theory is used to calculate the E_{eff}-vs-$A^{1/2}$ theory curve in Fig. 20 directly.[8,9] When combined with the MTS load and stiffness data, the elasticity analysis also allows hardness to be calculated as a function of load[9,14] (Fig. 19). This method of calculating hardness, in which the area of the indent is determined from unloading

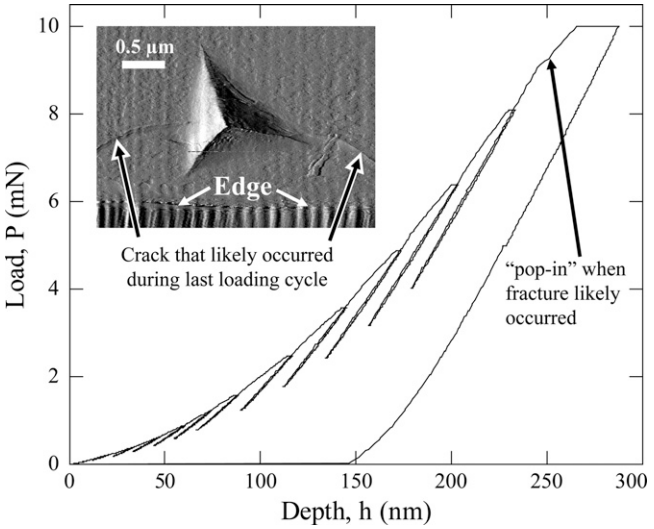

FIG. 22. Load–depth trace of multiload indent (Fig. 21) placed near edge (d = 0.9 μm) of SOI specimen. Inset: AFM image of multiload indent near edge (d = 0.9 μm) of SOI specimen.

stiffness based on elasticity theory, is a fundamentally different way of calculating area than used by the MTS instrument itself, which instead calculates area based on contact depth. Overall, the three methods of generating the data agree well. The agreement is good partly because there is little pileup in the indents, which, if present, would make the MTS areas estimated based on contact depth become unreliable.

To investigate the properties of the SOI near an edge, five multiload indents (P_0 = 10 mN, $A^{1/2} \approx 0.94$ μm^2) were placed near a free edge created by cleaving along a 100 surface. Data from one of these indents, in the form of a SYS plot with C_m = 2.7 μm/N already removed, are compared in Fig. 21 with Hysitron data taken from the center of the specimen. In this figure it becomes clear that the uncorrected data from the near-edge indent (solid circles) differ from the data from the specimen-center indents (crosses) simply by a line of constant slope. If we subtract a line of slope 1.7 μm/N from the near-edge data, we can get them to overlap the data from the center of the specimen (solid squares). The one exception to this rule is the datum at highest load from the near-edge indent, which is lower than it should be. This anomaly appears to be caused by the fracture of the silicon near this load (shown below). We immediately identify 1.7 μm/N as a structural compliance associated with the edge. We conclude, therefore, that even in layered specimens, edge effects can be handled using a structural compliance construction.

Examination of the AFM image of the near-edge indent (Fig. 22) reveals a crack that formed on the surface of the SOI during the experiment. A "pop-in" was observed to occur in the final partial loading segment of the load–depth trace, suggesting that the fracture event only affected the final loading and unloading segment, which is consistent with the odd behavior of the highest-load datum from the near-edge indent in Fig. 21. After correcting the SYS correlations of the five near-edge indents (d = 0.9, 1.7, 3.2, 14.4, and 16.3 μm) for C_s, the $J_0^{1/2}$ data at the lower loads can be compared to the specimen-center $J_0^{1/2}$ data to investigate any differences in properties at lower loads for the near-edge indent. No systematic trends are observed in the SYS data not affected by a fracture event, suggesting the properties of the SOI do not change as the cleaved edge is approached.

IV. SUMMARY AND FINAL COMMENTS

The SYS correlation has been used to account for C_s arising from edges in five separate materials systems:

(1) In a PMMA rod, the SYS correlation is used to account for C_s arising from a free edge in an effort to examine how E_s and H depend on proximity of the free edge. The edge itself is formed by the intersection between the test surface and the original, cylindrical surface of the extruded rod, so that the analysis allows us to examine how the properties of the PMMA change near the extruded surface. They remain constant to within about 15 μm of the surface. Closer than this, H decreases but E_s remains the same. In a control experiment, properties measured near another free edge created by slicing the specimen with a microtome do not show as great a decrease in H.

(2) In the CCML of loblolly pine, the SYS correlation reveals a negative C_s. The negative C_s results from the proximity of the surrounding cell walls which, by virtue of higher modulus, constrain the CCML.

(3) In the wood cell walls in a wood–polypropylene composite, nanoindentation is used to compare the properties of different cell wall fragments. The properties appear to differ between fragments when the standard analysis is used. However, when the SYS correlation is used to determine C_s it is found that one fragment has an anomalously high C_s. We conjecture that that a subsurface crack or other defect contributes to the high C_s for this fragment. When the different C_s are accounted for in the analysis, the properties of all cell wall fragments are revealed to be about the same.

(4) Nanoindentation is used to measure the properties of 3 to 10 μm diameter AlB_2 particles embedded in an aluminum matrix. The SYS correlation is used to remove the effects of the surrounding matrix. The analysis reveals systematic trends in properties depending on the orientations of the particles. Without the corrected analysis these trends are obscured.

(5) The properties of a SOI specimen are investigated using nanoindentation near a free edge of the specimen. Because of layering, the SYS plot is not a straight line; nevertheless, the shape of the SYS plot can be accounted for using elasticity theory. Even for this layered system, we find that it is possible to account for the specimen edge effect employing a C_s, which is independent of the size of the indent.

This use of the SYS plot approach for removing edge effects in nanoindentation shows much promise. This method apparently works because of the asymptotic behavior of the modulus of contact, which deviates linearly from E_{eff} (of the phase being tested) in proportion to $A^{1/2}/d$ for small $A^{1/2}/d$ (see Appendix). The other part of the SYS plot entails the hardness, which enters into the parameter ${J_0}^{1/2}$; and if the indent is placed close enough to the edge so that the hardness is modified, then the analysis must break down. In practice, this problem can be avoided in experiments by making sure that the indents are made sufficiently small that their plastic zones do not come too close to the edge. For fused silica, with $H/E \approx 0.15$ and therefore a small plastic zone, indents can be placed as close to the edge of the specimen as $d = 0.8\ A^{1/2}$, yet the analysis still works[5] and the hardness remains unaffected. For PMMA studied here, with a lower H/E ratio and therefore larger plastic zone than fused silica, the hardness values appear to be influenced by the edge at $d \approx 1.3\ A^{1/2}$ according to Fig. 8, where there is an indication that the hardness drops for the data from the microtomed edge. A way to use the SYS plot approach to prevent problems with overlap between the plastic zone and edge is to rely on the zero-load limit, where ${C_t P_0}^{1/2}$ extrapolates to the intercept ${J_0}^{1/2}$ ($P_0 = 0$). This intercept should be free of the kinds of artifacts we consider here.

Using the SYS correlation to remove edge artifacts is easiest if the material has no indentation size effect, in which case the data form a straight line whose slope is $C_m + C_s$. If instead there is a size effect in either hardness or modulus then the data will no longer form a straight line or, if the size effect is subtle, the data will form a straight line but the slope will be wrong. Of the specimens studied here only the SOI possesses a significant size effect, and because this effect is mostly in the modulus we can get around any difficulties by being able to accurately model E_{eff}. In situations where the size effect is in H, it should still be possible to apply the SYS plot to separate out the artifact by examining the systematic trend of the data as a function of position away from the edge and by extrapolating the data to low load.

ACKNOWLEDGMENTS

The study of AlB_2 is based on work supported by the National Science Foundation under Grant No. 0351449 (PREM Program). Research on PMMA was sponsored by the National Science Foundation (Award CMS-0528073).

REFERENCES

1. W.C. Oliver and G.M. Pharr: Improved technique for determining hardness and elastic modulus using load and displacement sensing indentation experiments. *J. Mater. Res.* **7**(6), 1564 (1992).
2. I.N. Sneddon: Relation between load and penetration in axisymmetric Boussinesq problem for punch of arbitrary profile. *Int. J. Eng. Sci.* **3,** 47 (1965).
3. A. Bolshakov and G.M. Pharr: Inaccuracies in Sneddon's solution for elastic indentation by a rigid cone and their implications for nanoindentation data analysis, in *Thin Films: Stresses and Mechanical Properties VI*, edited by W.W. Gerberich, H. Gao, J.E. Sundgren, and S.P. Baker (Mater. Res. Soc. Symp. Proc. **436,** Pittsburgh, PA, 1997), p. 189.
4. M. Troyon and S. Lafaye: About the importance of introducing a correction factor in the Sneddon relationship for nanoindentation measurements. *Philos. Mag.* **86**(33–35), 5299 (2006).
5. J.E. Jakes, C.R. Frihart, J.F. Beecher, R.J. Moon, and D.S. Stone: Experimental method to account for structural compliance in nanoindentation measurements. *J. Mater. Res.* **23**(4), 1113 (2008).
6. R.B. King: Elastic analysis of some punch problems for a layered medium. *Int. J. Solids Struct.* **23**(12), 1657 (1987).
7. M.F. Doerner and W.D. Nix: A method for interpreting the data from depth-sensing indentation instruments. *J. Mater. Res.* **1**(4), 601 (1986).
8. D.S. Stone: Elastic rebound between an indenter and a layered specimen. I. Model. *J. Mater. Res.* **13**(11), 3207 (1998).
9. K.B. Yoder, D.S. Stone, R.A. Hoffman, and J.C. Lin: Elastic rebound between an indenter and a layered specimen. II. Using contact stiffness to help ensure reliability of nanoindentation measurements. *J. Mater. Res.* **13**(11), 3214 (1998).
10. A.C. Fischer-Cripps: Critical review of analysis and interpretation of nanoindentation test data. *Surf. Coat. Technol.* **200**(14–15), 4153 (2006).
11. W.C. Oliver and G.M. Pharr: Measurement of hardness and elastic modulus by instrumented indentation: Advances in understanding and refinements to methodology. *J. Mater. Res.* **19**(1), 3 (2004).
12. Y-T. Cheng and C-M. Cheng: Scaling, dimensional analysis, and indentation measurements. *Mater. Sci. Eng., R* **44**(4–5), 91 (2004).
13. A.A. Elmustafa, S. Kose, and D.S. Stone: The strain-rate sensitivity of the hardness in indentation creep. *J. Mater. Res.* **22**(4), 926 (2007).
14. D.S. Stone, K.B. Yoder, and W.D. Sproul: Hardness and elastic modulus of TiN based on continuous indentation technique and new correlation. *J. Vac. Sci. Technol. A* **9**(4), 2543 (1991).
15. D.L. Joslin and W.C. Oliver: New method for analyzing data from continuous depth-sensing microindentation tests. *J. Mater. Res.* **5**(1), 123 (1990).
16. M. Sakai and Y. Nakano: Elastoplastic load–depth hysteresis in pyramidal indentation. *J. Mater. Res.* **17**(8), 2161 (2002).
17. N.A. Stilwell and D. Tabor: Elastic recovery of conical indentations. *Proc. Phys. Soc.* **78,** 169 (1961).
18. N.B. Duque, Z.H. Melgarejo, and O.M. Suarez: Functionally graded aluminum matrix composites produced by centrifugal casting. *Mater. Charact.* **55**(2), 167 (2005).
19. Z.H. Melgarejo, O.M. Suarez, and K. Sridharan: Wear resistance of a functionally-graded aluminum matrix composite. *Scr. Mater.*, **55**(1 Spec), 95 (2006).
20. Z.H. Melgarejo, O.M. Suarez, and K. Sridharan: Microstructure and properties of functionally graded Al–Mg–B composites

fabricated by centrifugal casting. *Compos. Part A: Appl. Sci. Manuf.* **39**(7), 1150 (2008).
21. N. Miller, K. Tapily, H. Baumgart, G.K. Cellar, F. Brunier, and A.A. Elmustafa: Nanomechanical properties of strained silicon-on-insulator (SOI) films epitaxially grown on $Si_{1-x}Ge_x$ and layer transferred wafer bonding, in *Surface and Interfacial Nanomechanics*, edited by R.F. Cook, W. Ducker, I. Szlufarska, and R.F. Antrim (Mater. Res. Soc. Symp. Proc. **1021E**, Warrendale, PA, 2007), 1021-HH05-24.
22. R. Wimmer, B.N. Lucas, T.Y. Tsui, and W.C. Oliver: Longitudinal hardness and Young's modulus of spruce tracheid secondary walls using nanoindentation technique. *Wood Sci. Technol.* **31**(2), 131 (1997).
23. C.E. Gerber: *Contact Problems for the Elastic Quarter-Plane and for the Quarter Space* (Stanford University, Palo Alto, CA, 1968), p. 100.
24. S.S. Chiang, D.B. Marshall, and A.G. Evans: The response of solids to elastic/plastic indentation. I. Stresses and residual stresses. *J. Appl. Phys.* **53**(1), 298 (1982).
25. K.L. Johnson: *Contact Mechanics* (Cambridge University Press, Cambridge, UK, 1985), p. 452.
26. C. Deppisch, G. Liu, J.K. Shang, and J. Economy: Processing and mechanical properties of AlB2 flake reinforced Al-alloy composites. *Mater. Sci. Eng., A* **A225**(1–2), 153 (1997).
27. K. Liu, X.L. Zhou, X-R. Chen, and W-J. Zhu: Structural and elastic properties of AlB2 compound via first-principles calculations. *Physica B (Amsterdam)* **388**(1–2), 213 (2007).
28. J.J. Vlassak and W.D. Nix: Measuring the elastic properties of anisotropic materials by means of indentation experiments. *J. Mech. Phys. Solids* **42**(8), 1223 (1994).
29. M. Hetenyi: Method of solution for elastic quarter-plane. *ASME Trans. J. Appl. Mech. Ser. E, J. Appl. Mech.* **27**(2), 289 (1960).
30. M. Hetenyi: *A general solution for the elastic quarter space. Trans. ASME Ser. E., J. Appl. Mech.* **37**(1), 70 (1970).
31. L.M. Keer, J.C. Lee, and T. Mura: Hetenyi's elastic quarter space problem revisited. *Int. J. Solids Struct.* **19**(6), 497 (1983).
32. L.M. Keer, J.C. Lee, and T. Mura: A contact problem for the elastic quarter space. *Int. J. Solids Struct.* **20**(5), 513 (1984).
33. G.Y. Popov: An exact solution of the mixed elasticity problem in a quarter-space. *Mech. Solids* **38**(6), 23 (2003).
34. N. Schwarzer, I. Hermann, T. Chudoba, and F. Richter: Contact modelling in the vicinity of an edge. *Surf. Coat. Techol.* **146–147**, 371 (2001).

APPENDIX: PHYSICAL SIGNIFICANCE OF C_S FOR AN INDENT PLACED NEAR AN EDGE

Edge problems have been studied by a few researchers within the context of the quarter-space problem (e.g., Refs. 23, 29–34). Gerber's solution[23] for elastic contact against an elastic quarter space [free edge problem, Fig. 1(a)] has already been shown to give rise to a structural compliance of the form of Eq. (6) with f = constant.[5] Here, we employ a physical argument to suggest the same is true for the more general edge problem.

Figure A1 illustrates schematically the effect of an interface or edge on the stiffness of contact between an indenter and specimen. The total compliance of contact between indenter and specimen is $C_p + C_s$, so the modulus of contact between indenter and specimen is $[(C_p + C_s)A^{1/2}]^{-1}$, which serves as the vertical axis in Fig. A1. For a given indenter shape and orientation with respect

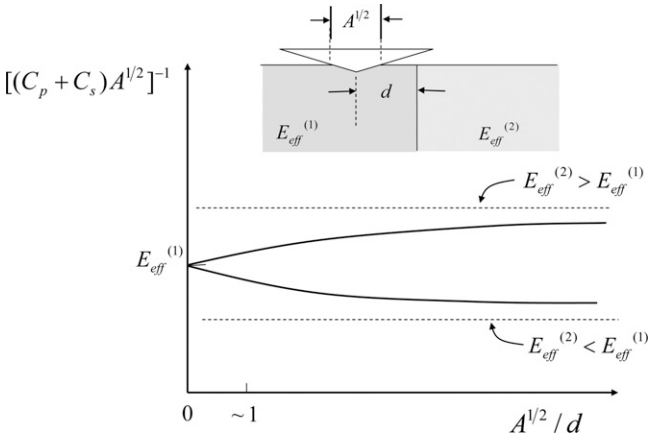

FIG. A1. Dependence of modulus of contact, $[(C_p + C_s)\,A^{1/2}]^{-1}$, on $A^{1/2}/d$ for indents placed near a heterophase interface.

to the edge, this modulus depends on the ratio $A^{1/2}/d$, the horizontal axis. We suppose that if the indent were placed in phase 1 far from the interface, the limiting value of $[(C_p + C_s)A^{1/2}]^{-1}$ would be $E_{eff}^{(1)}$, whereas if the indent were placed in phase 2 far from the interface, the limiting value would be $E_{eff}^{(2)}$. If phase 2 is a vacuum, then $E_{eff}^{(2)} = 0$.

For the purpose of discussion, suppose that the center of the indent is placed in phase 1 at some distance d from the interface or edge. If phase 2 is stiffer than phase 1, then the modulus of contact will increase as $A^{1/2}/d$ is made larger. If phase 2 is more compliant than phase 1, then the modulus of contact will be lowered if $A^{1/2}/d$ is made larger. In the limit that the indent is large enough to straddle the edge ($A^{1/2}/d > 1$ in Fig. A1), the modulus measurement will move toward a property that is intermediate between the properties on either side of the interface. We represent the behavior of the modulus of contact with the solid lines in Fig. A1 and assume that their behaviors are monotonic. For small $A^{1/2}/d$, we suppose that the modulus of contact varies as

$$\left[(C_p + C_s)A^{1/2}\right]^{-1} \approx E_{eff}^{(1)} \pm E' \times \left(\frac{A^{1/2}}{d}\right)^{w} \quad , \quad \text{(A1)}$$

where E' is a (positive) constant having units of Young's modulus, and w is a power that we will presently evaluate. If phase 2 is stiffer than phase 1, then a (+) sign is used for the second term, whereas if phase 2 is more compliant a (−) sign is used. If we solve for the compliances in Eq. (A1) then, using $1/(1 \pm x) \approx 1 \mp x$, we have

$$C_p + C_s \approx \frac{1}{E_{eff}^{(1)} A^{1/2}} \mp \frac{E'}{\left(E_{eff}^{(1)}\right)^2 A^{1/2}} \times \left(\frac{A^{1/2}}{d}\right)^{w} \quad . \quad \text{(A2)}$$

Here, the (−) sign is used if the nearby phase 2 is stiffer than phase 1, and the (+) sign is used if phase 2 is more compliant. The first term in Eq. (A2) we attribute to

the behavior of phase 1 when an indent is placed far from the interface, whereas the second term is attributed to the interface. The second term means that if, for a given load and area, an indent is placed near the interface, the displacement will be decreased if the second phase is stiffer than the first phase or increased if the second phase is more compliant than the first. Moreover, in the limit $A^{1/2}/d \rightarrow 0$ we know by St. Venant's principle that this extra displacement must not depend on $A^{1/2}$. Therefore $w = 1$, and

$$C_p + C_s \approx \frac{1}{E_{eff}^{(1)} A^{1/2}} \mp \frac{E'}{\left(E_{eff}^{(1)}\right)^2} \frac{1}{d} \quad . \qquad \text{(A3)}$$

In conclusion, the compliance of contact between indenter and specimen near an interface can be approximated using Eq. (A3). From Fig. A1, E' in this formula scales in proportion to $E_{eff}^{(2)} - E_{eff}^{(1)}$. The first term on the right-hand side corresponds to C_p, and the second term on the right-hand is the structural compliance, C_s, arising from the interface. C_s is positive if the neighboring phase is more compliant and is negative if the neighboring phase is stiffer than the phase being tested. Although this equation is in principle an approximation valid for $A^{1/2}/d \rightarrow 0$, our measurements suggest it works well even for $A^{1/2}/d$ approaching 1, that is, when the indent almost touches the edge.